Pure Appl. Geophys. 175 (2018), 2955–2973

https://doi.org/10.1007/s00024-018-1809-x

Pure and Applied Geophysics

Subsurface Investigation of the Neogene Mygdonian Basin, Greece Using Magnetic Data

Ismael M. Ibraheem,[1] Marcus Gurk,[1] Nikolaos Tougiannidis,[2] and Bülent Tezkan[1]

Abstract—A high-resolution ground and marine magnetic survey was executed to determine the structure of the subsurface and the thickness of the sedimentary cover in the Mygdonian Basin. A spacing of approximately 250 m or 500 m between measurement stations was selected to cover an area of 15 km × 22 km. Edge detectors such as total horizontal derivative (THDR), analytic signal (AS), tilt derivative (TDR), enhanced total horizontal gradient of tilt derivative (ETHDR) were applied to map the subsurface structure. Depth was estimated by power spectrum analysis, tilt derivative, source parameter imaging (SPI), and 2D-forward modeling techniques. Spectral analysis and SPI suggest a depth to the basement ranging from near surface to 600 m. For some selected locations, depth was also calculated using the TDR technique suggesting depths from 160 to 400 m. 2D forward magnetic modeling using existing boreholes as constraints was carried out along four selected profiles and confirmed the presence of alternative horsts and grabens formed by parallel normal faults. The dominant structural trends inferred from THDR, AS, TDR, and ETHDR are N–S, NW–SE, NE–SW and E–W. This corresponds with the known structural trends in the area. Finally, a detailed structural map showing the magnetic blocks and the structural architecture of the Mygdonian Basin was drawn up by collating all of the results.

Key words: Mygdonian Basin, magnetic data, edge detection, TDR, AS, SPI, ETHDR, 2D forward modeling.

1. Introduction

The Mygdonian Basin is considered one of the most seismically active zones in northern Greece and the surrounding region. It is located about 30 km northeast of the city of Thessaloniki, between Lake Volvi and Lake Langada (Fig. 1). The EUROSEISTEST facility was constructed as a test site in the middle of the Mygdonian Basin in 1993. A strong earthquake ($M = 7.1$R to $M = 6.02$R, Manakou et al. 2007) had occurred there on June 20, 1978. The test site, between the villages of Profitis and Stivos, monitors soil–soil and soil–construction interactions during seismic events (Makra and Chavez-Garcia 2016).

The basin has been studied by many authors: a 3D model of the basin based on P-wave refraction, electrical soundings and drillings was created by Bureau de Recherche Geologiques et Minieres (BRGM) (BRGM 1971) and Manakou et al. (2010). In this model, the bedrock between Lake Langada and Lake Volvi forms a syncline with an E–W axis. The deepest point with a depth of 400 m is located in the western part of the area. Hatzfeld et al. (1987) identified three groups of faults using focal mechanisms: normal faults with a sinistral strike-slip component on NW–SE trending planes, dextral strike-slip faults on NNE-SSW trending planes, and normal faults on roughly E–W trending planes. Using aeromagnetic data, Stampolidis and Tsokas (2002) found that the Curie-depth estimates for Macedonia and Thrace range from 11.2 to 17.3 km. The area was also examined in several electromagnetic studies (Gurk et al. 2008; Bastani et al. 2011; Autio et al. 2016; Widodo et al. 2016) to map the top of the basement and provide information about the fault pattern. However, accurate mapping of the bedrock by electromagnetic methods is quite difficult due to the screening effects of highly conductive overlying sediments (Autio et al. 2016). Depth data from many drilling wells that reached the basement rocks (Table 1) inside the Mygdonian Basin were collected after Veranis (2010) and served as constraints to model the surface of the basement.

[1] Institute of Geophysics and Meteorology, University of Cologne, Pohligstrsse 3 (Office 3.235), 50969 Cologne, Germany. E-mail: ismail.geo@gmail.com; ismael.ibraheem@geo.uni-koeln.de

[2] Institute of Geology and Mineralogy, University of Cologne, Zülpicher Str. 49a, 50674 Cologne, Germany.

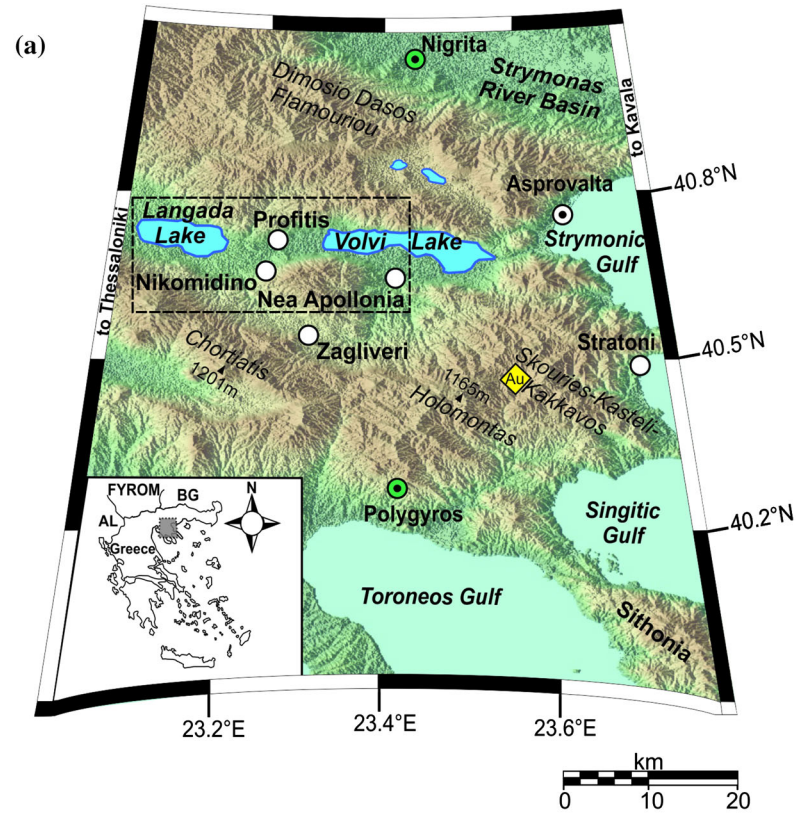
(a)
Nigrita
Strymonas River Basin
Dimosio Dasos Flamouriou
to Kavala
Asprovalta
40.8°N
Langada Lake
Profitis
Volvi Lake
Strymonic Gulf
to Thessaloniki
Nikomidino
Nea Apollonia
Zagliveri
Stratoni
40.5°N
Chortiatis
1201m
1165m
Holomontas
Skouries-Kastelli-Kakkavos
AU
FYROM
BG
AL
Greece
N
Polygyros
Singitic Gulf
40.2°N
Toroneos Gulf
Sithonia
23.2°E
23.4°E
23.6°E
km
0
10
20

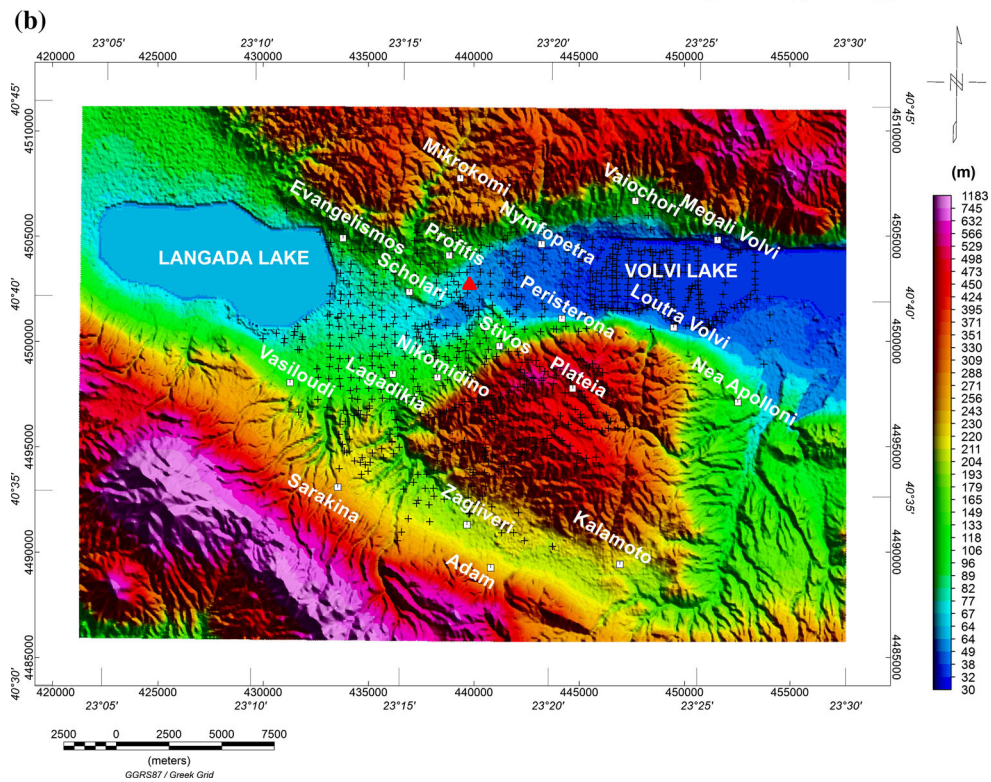
(b)
LANGADA LAKE
VOLVI LAKE
Mikrokomi
Vaiochori
Megali Volvi
Evangelismos
Nymfopetra
Profitis
Scholari
Peristerona
Loutra Volvi
Stivos
Nikomidino
Vasiloudi
Lagadikia
Platela
Nea Apolloni
Sarakina
Zagliveri
Kalamoto
Adam
(m)
1183
745
632
566
529
498
473
450
424
395
371
351
330
309
288
271
256
243
230
220
211
204
193
179
165
149
133
118
106
96
89
82
77
67
64
64
49
38
32
30
2500 0 2500 5000 7500
(meters)
GGRS87 / Greek Grid

◀Figure 1
a Location of the survey area in northern Greece, between Lake Langada and Lake Volvi. **b** Topographic map of the study area. The 90 m resolution Shuttle Radar Topography Mission data (SRTM) were used to construct the map. Black crosses indicate the locations of the magnetic stations, white squares represent the villages, and red triangle represents the location of the reference magnetic station

The objective of the present magnetic survey was to obtain a high-resolution data set of the study area in order to enhance our understanding of the distribution of sedimentary cover and the depth of the basement. It also aimed to throw some light on the subsurface structure of the Mygdonian Basin and assess the site effect in the area around the EUROSEISTEST station. In this regard, the data were used to map contacts and structural features within the study area.

2. Geology and Tectonic Setting

Two major tectonic phenomena are observed in the northern part of the Aegean region which includes the Mygdonian Basin: the N–S extension of the Aegean Sea and the western termination of the North Anatolian strike-slip fault (Dewey and Sengör 1979). A geological and structural map of the Mygdonian Basin is shown in Fig. 2.

Table 1

Boreholes reaching the basement rocks (Veranis 2010)

X	*Y*	Borehole name	Depth to bedrock (m)
431,557	4,498,612	62	140
431,293	4,499,231	63	146
436,120	4,497,971	75	110
439,307	4,499,376	80	132
443,522	4,500,504	86	0
443,051	4,505,511	91	12
442,760	4,505,559	92	0
441,088	4,503,955	93	78
439,625	4,503,649	94	20
438,553	4,505,005	96	138
438,400	4,504,454	97	77
433,875	4,504,580	102	22
445,313	4,503,940	GGEO	150
443,602	4,501,468	GP2	180
442,734	4,501,161	GP3	120

Mygdonia valley is located on the border of two geotectonic zones (Jacobshagen 1986): the Circum-Rhodope-Belt (CRB) to the west (between the Axios and Strimon rivers) and the Serbo-Macedonian Massif (SMM) to the east (Manakou et al. 2007).

The crystalline basement of the basin consists mainly of gneiss, amphibolites, schist, marble intrusions, and granites. It is exposed towards the northern and southern edges and deepens towards the center of the basin (Kockel et al. 1971; Manakou et al. 2010). The sediments filling the basin can be classified into two main units: the lower unit where the pre-Mygdonian system was deposited during the Neogene and the upper unit where the Mygdonian system was deposited into the younger grabens during the Quaternary (Pleistocene to Holocene). The pre-Mygdonian system is made up of conglomerates, sandstones, silt–sand sediments, and red-beds, whereas the Mygdonian system comprises fluviolacustrine, deltaic, lacustrine, lagoonal, and estuarine deposits (Psilovikos 1977; Psilovikos and Sotiriadis 1983).

A series of grabens with E–W to NW–SE trends were formed in the SMM by normal faulting during the Neogene and Quaternary. The Mygdonian Basin is the remnant of one of these grabens (Karagianni et al. 1999). The central and eastern parts of the basin belong to the SMM, while the western part belongs to the CRB (Manakou et al. 2007). The main regional fault trend in the area is oriented NW–SE, whereas the trends of other faults are E–W and N–S. These trends coincide with the known main tectonic line in northern Greece (Raptakis et al. 2005). The main tectonic fault system of the Mygdonian Basin is, however, the roughly E–W trending 12 km-long Vasiloudi–Gerakarou–Nikomidino–Stivos–Peristerona (F-GNSP) fault (Fig. 2). The F-GNSP fault which has two branches: F-VL and F-Sx, runs along the southern border of the basin from the village of Vasiloudi to the village of Peristerona with a 70°–80°N dip (Manakou et al. 2010).

The occurrence of carbon-rich hot springs in Lake Volvi (Loutra Volvi) and several tufa towers (Fig. 3) on the northern rim of the basin (between Stivos and Profitis; Nymphopetra) as well as along the F-GNSP fault (Tranos et al. 2003; Raptakis et al. 2005) suggest that the tufa genesis is connected with the faults in the basement. Tufa deposits are preferentially

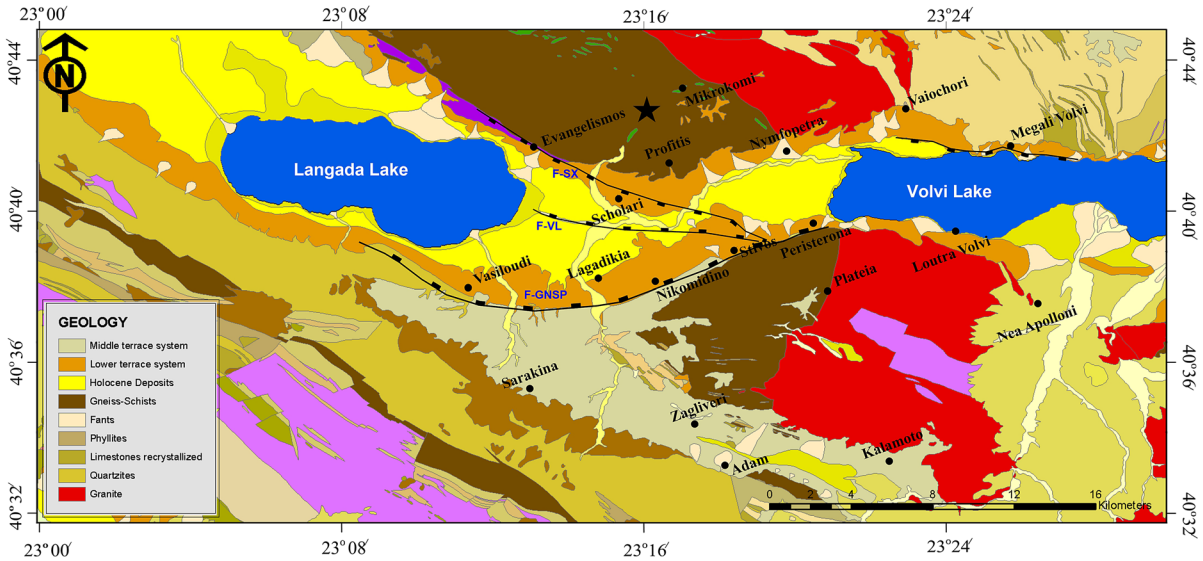

Figure 2
Geological and structural map of the Mygdonian Basin. The thick solid lines indicate the main fault (F-GNSP) and its branches (F-VL and F-Sx) in addition to other faults in the area. The star depicts the epicenter of the 1978 earthquake. This map is reconstructed after Thanassoulas et al. (1987), Cheng et al. (1994) and Manakou et al. (2010)

located along fracture traces, either immediately above extensional fissures or in the hanging wall of normal faults. Therefore, the tufa pattern at the surface may delineate the fault distribution at depth and indicate areas with increased basement fracturation (Hancock et al. 1999).

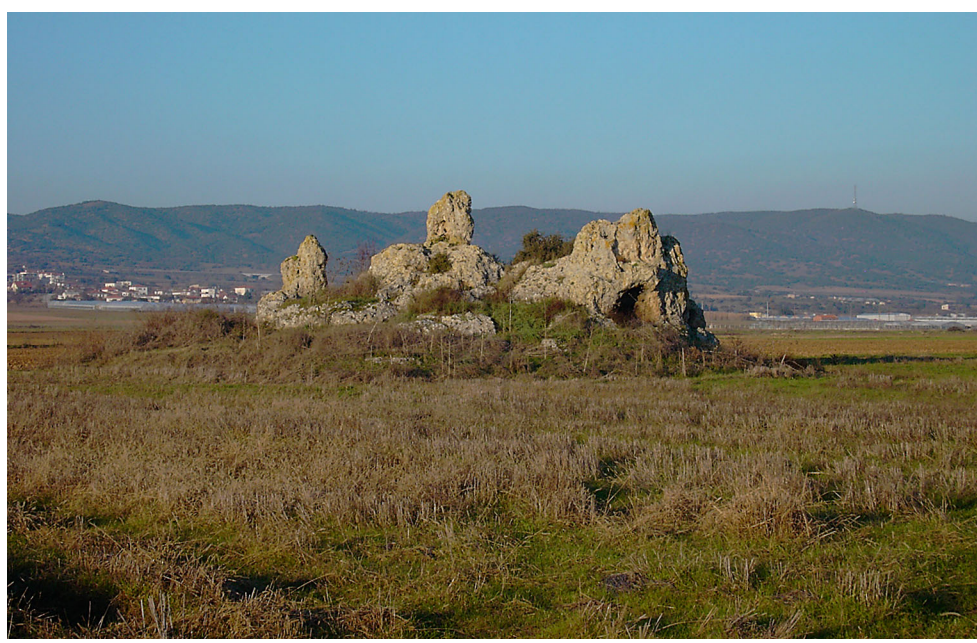

Figure 3
Field photography shows tufa cones in the northern part of the Mygdonian Basin. View to the northeast with the village of Profitis in the background

3. Magnetic Survey

Since it was first used in geophysical exploration, the use of the magnetic method has expanded from a focus on localized studies such as mineral exploration to its use as a regional tool for mapping the thickness of sedimentary basins as well as the geological structure and nature of buried crystalline rocks (Hinze et al. 2013).

During several campaigns, a high-resolution ground magnetic survey was carried out, using the Gem-system GSM-19T Proton Magnetometer to sample the total magnetic field along the profiles at intervals of 500 m. It has a 0.05 nT sensitivity and a large memory storage of 32 Mbytes. The sensor was set at a height of 2.8 m. A Geometrics G-856AX Magnetometer with a large sensor head was used as a base station at the EUROSEISTEST, sampling the total magnetic field every 60 s to measure the diurnal variations. A marine magnetic survey was also conducted in the western part of Lake Volvi using the Gem-System GSM-19T Proton Magnetometer. Magnetic susceptibilities were measured for typical rock outcrops (336 readings) using a SM30 magnetic susceptibility meter.

The total magnetic field values recorded at the stations were corrected for the diurnal variations. The data were then inspected visually; spikes were removed manually to construct a total magnetic intensity (TMI) map (Fig. 4a). The Definitive Geomagnetic Reference Field (DGRF) values were then subtracted from the TMI values. Finally, the TMI values were gridded and reduced to the north magnetic pole using the Geosoft Oasis Montaj software (2008). A value of 57.57° was used for the inclination and the value of 3.77° for the declination—assuming only induced magnetization—to overcome the skewness caused by the inclination of the earth's magnetic field and to re-position magnetic anomalies directly over their sources.

The TMI reduced to the pole (Fig. 4b) exhibits a major high magnetic belt extending from the southwestern to the northeastern parts of the area and trending NE–SW with a maximum magnetic value of 70 nT near the village of Vaiochori. Two low negative magnetic belts can also be identified on the "reduced-to-the pole" (RTP) magnetic map: one is located in the southwestern corner of the survey area and trending NW–SE with a minimum magnetic value of – 162 nT near Vasiloudi. The second is in the northwest and is trending NE–SW, parallel to the high magnetic belt with some high magnetic anomalies in the area around Scholari and Profitis. Those magnetic anomalies inside the previous magnetic belts are generally trending N–S, NW–SE, and NNW–SSE, and could be associated with shallow basement structures and/or igneous intrusions.

4. Spectral Analysis as a Tool for Regional–Residual Separation and Depth Estimation

Several authors have used the power spectrum technique to determine the depth of subsurface magnetic sources (Bhattacharyya 1965, 1966; Cassano and Rocca 1975; Spector and Grant 1970; Connard et al. 1983; Fedi et al. 1997; Saade 2016; Ibraheem et al. 2018). The Fast Fourier Transform (FFT) was applied to the RTP magnetic grid to calculate the 2D radially averaged energy–power spectrum curve. The 2D power spectrum of the present magnetic data (Fig. 5a) shows three straight segments related to deep, intermediate, and shallow magnetic sources. The inspection of the curve can give us a good idea about the depth of magnetic sources in the survey area. Depth values can be calculated from the slope (S) of a straight line interpolating the diagram of the log-power versus the wavenumber using the following formula (Hinze et al. 2013):

$$\text{Depth Z} = -(S)/4\pi.$$

Depth computations performed on these segments—assuming random magnetization—show that the average depth from the survey level to the top of deep, intermediate, and shallow magnetic sources is 2.0, 0.6, and 0.3 km, respectively.

A regional–residual separation of the magnetic components was performed using an interactive power spectrum filter. First, the RTP magnetic data was continued upwards to a height of 100 m above ground. The high frequency component (beyond Nyquist frequency) was then removed using a low-pass filter with a cutoff wavenumber of 1 km^{-1}.

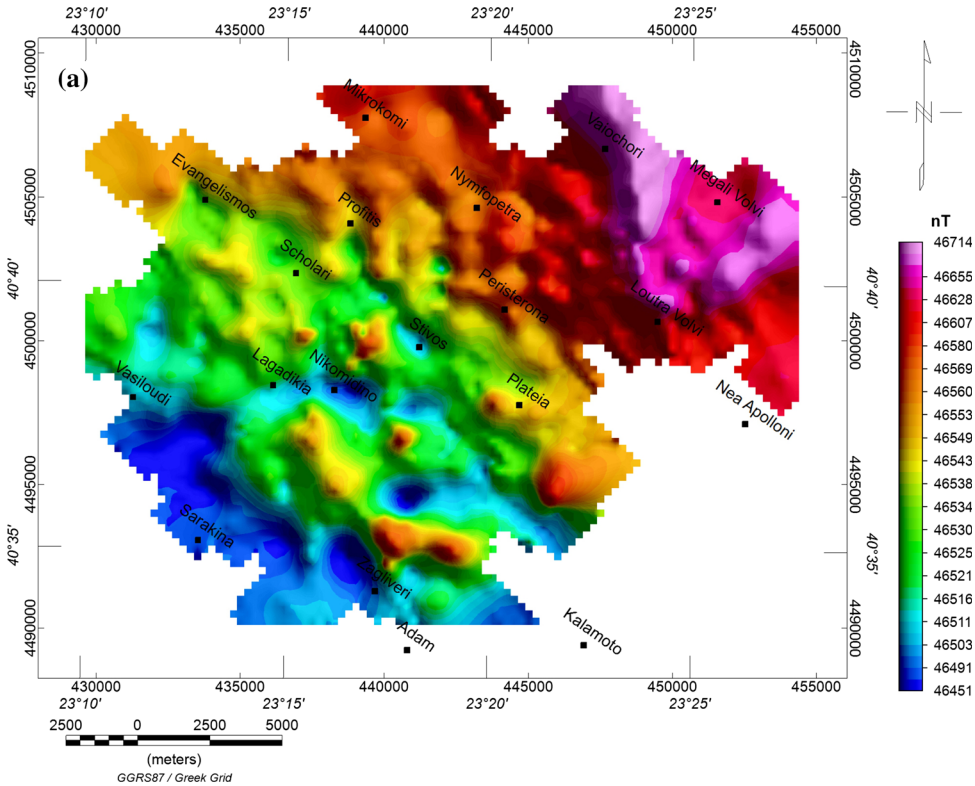
(a)
Mikrokomi
Vaiochori
Megali Volvi
Evangelismos
Nymfopetra
Profitis
Scholari
Peristerona
Loutra Volvi
Stivos
Lagadikia
Nikomidino
Plateia
Vasiloudi
Nea Apolloni
Sarakina
Zagliveri
Adam
Kalamoto
nT
46714
46655
46628
46607
46580
46569
46560
46553
46549
46543
46538
46534
46530
46525
46521
46516
46511
46503
46491
46451
23°10'
23°15'
23°20'
23°25'
430000
435000
440000
445000
450000
455000
4510000
4505000
4500000
4495000
4490000
40°40'
40°35'
2500 0 2500 5000
(meters)
GGRS87 / Greek Grid

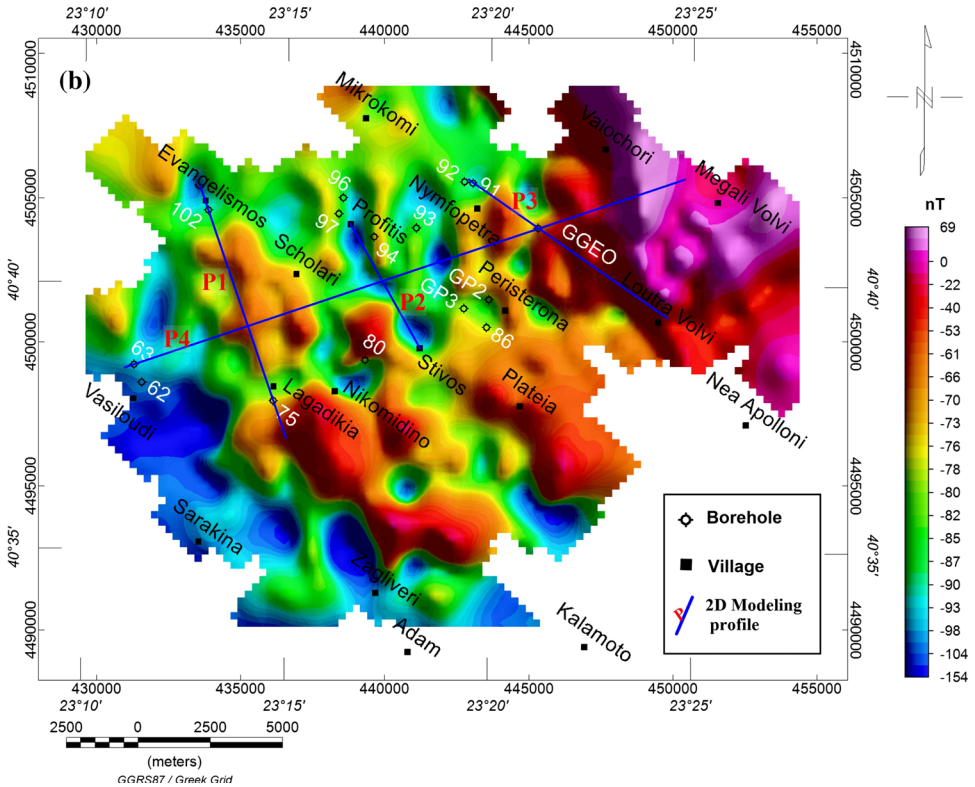
(b)
Mikrokomi
Vaiochori
Megali Volvi
Evangelismos
Nymfopetra
Profitis
Scholari
Peristerona
Loutra Volvi
Stivos
Lagadikia
Nikomidino
Plateia
Vasiloudi
Nea Apolloni
Sarakina
Zagliveri
Adam
Kalamoto
P1
P2
P3
P4
GGEO
GP2
GP3
102
96
97
94
93
92
91
86
80
63
62
75
Borehole
Village
2D Modeling profile
nT
69
0
-22
-40
-53
-61
-66
-70
-73
-76
-78
-80
-82
-85
-87
-90
-93
-98
-104
-154
23°10'
23°15'
23°20'
23°25'
430000
435000
440000
445000
450000
455000
4510000
4505000
4500000
4495000
4490000
40°40'
40°35'
2500 0 2500 5000
(meters)
GGRS87 / Greek Grid

◀Figure 4
Total intensity magnetic map of Mygdonian Basin **(a)**, RTP total intensity magnetic map **(b)**

Regional and residual magnetic maps were calculated using high- and low-pass filters with a cutoff wavenumber of 0.17 km^{-1}. The cutoff wavenumbers were derived from the radially averaged power spectrum (Fig. 5a). The regional RTP magnetic map (Fig. 5b) is related to deeper sources and basement structures. It reflects two main regional trends in the area: NW–SE and NE–SW. The high magnetic anomaly belt in the central and eastern parts of the study area may reflect an uplift of the basement. The residual RTP magnetic map (Fig. 5c) depicts structural features at shallow depths and different anomaly trends such as N–S, NE–SW and E–W.

5. Edge Detection Techniques

5.1. Total Horizontal Derivative (THDR)

The total horizontal derivative (horizontal gradient) method, which has been used intensively to locate boundaries of susceptibility contrasts from magnetic data, states that the horizontal gradient of the anomaly caused by a tabular body tends to overlie the edges of the body if the edges are vertical and well-separated from each other (Cordell and Grauch 1985).

The greatest advantage of the horizontal gradient method is that it is less sensitive to noise in the data, because it only requires the calculations of the two first-order horizontal derivatives of the field (Phillips 1998). The method is also robust in delineating both shallow and deep magnetic sources, in comparison with the vertical gradient method which is useful in identifying shallower structures. The amplitude of the horizontal gradients is expressed by:

$$\mathrm{THDR} = \sqrt{\left(\frac{\partial H}{\partial x}\right)^2 + \left(\frac{\partial H}{\partial y}\right)^2}$$

where $(\partial H/\partial x)$ and $(\partial H/\partial \mathrm{y})$ are the horizontal derivatives of the magnetic field in the x- and y-directions.

The THDR technique was applied to the magnetic data of the Mygdonian Basin to determine the boundaries of magnetic sources by tracing the contacts of magnetic susceptibility contrasts. The total horizontal map of the magnetic data (Fig. 6a) shows that the survey area is dissected by major faults striking in N–S, NW–SE, and NE–SW trends. High positive anomalies in the southern part of the map reflect surface and/or shallow subsurface magnetic sources. Another high anomaly located in Lake Volvi can also be interpreted as a shallow basement uplift.

5.2. Analytic Signal (AS) (Total Gradient)

The function used in the analytic method is the analytic signal amplitude of the potential field defined by Marson and Klingele (1993):

$$|A(x,y)| = \sqrt{\left(\frac{\partial H}{\partial x}\right)^2 + \left(\frac{\partial H}{\partial y}\right)^2 + \left(\frac{\partial H}{\partial z}\right)^2}$$

where $|A(x,y)|$ is the amplitude of the analytic signal at (x, y), H is the observed magnetic field at (x, y), and $(\partial H/\partial x, \partial H/\partial y, \partial H/\partial z)$ are the two horizontal and vertical derivatives of the observed field, respectively.

The maxima of AS are very useful for delineating edges of magnetic sources, because the AS amplitude peaks over magnetic sources. The maxima of AS of the magnetic data produce a clear resolution for the shallow bodies, but do not delineate deeper bodies very well (Arisoy and Dikmen 2013). Like the horizontal gradient method, the assumption of thick sources in the AS maps leads to minimum depth estimates. The analytic signal method is more susceptible to noise than the horizontal gradient method, as it requires the computation of the vertical derivative. It can be used to determine the position of the contrast, but not its sign since the amplitude of the analytic signal is always positive.

The analytic signal of the RTP magnetic data was calculated (Fig. 6b). Peaks of the analytic signal are in agreement with the location of the main fault F-GNSP in the area extending from Vasiloudi to Peristerona and may continue to Loutra Volvi (see Fig. 2). Many other significant magnetic

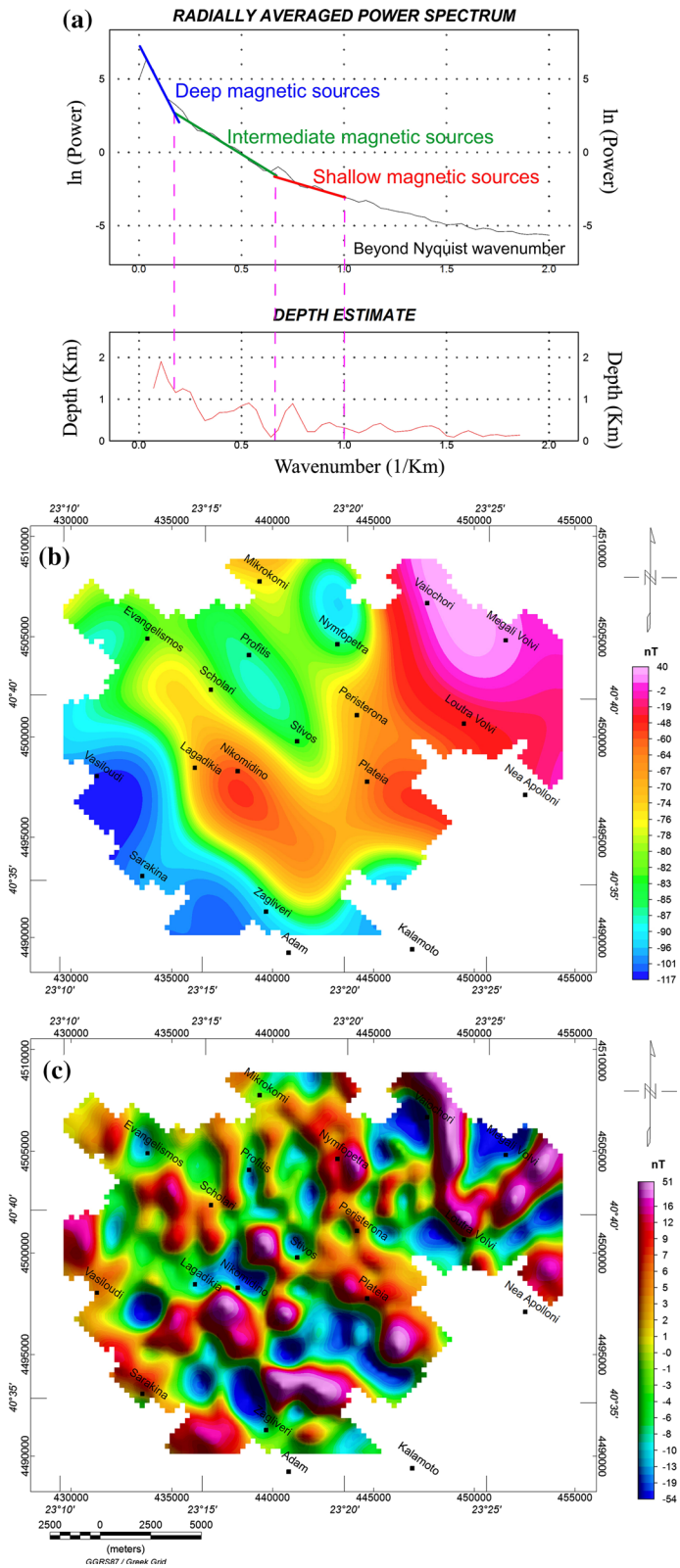
(a)
RADIALLY AVERAGED POWER SPECTRUM
Deep magnetic sources
Intermediate magnetic sources
Shallow magnetic sources
Beyond Nyquist wavenumber
ln (Power)
DEPTH ESTIMATE
Depth (Km)
Wavenumber (1/Km)
(b)
(c)
Mikrokomi
Valochori
Megali Volvi
Evangelismos
Nymfopetra
Profitis
Scholari
Peristerona
Loutra Volvi
Stivos
Lagadikia
Nikomidino
Plateia
Nea Apolloni
Vasiloudi
Sarakina
Zagliveri
Adam
Kalamoto
nT
(meters)
GGRS87 / Greek Grid

◀Figure 5
2D radially averaged power spectrum curve **(a)** Low-pass filtered regional RTP magnetic map **(b)** High-pass filtered residual RTP magnetic map **(c)**

susceptibility contacts/faults can be identified on the AS map, some of which can be considered as branches of the F-GNSP fault. Many magnetic intrusive bodies can also be seen in the AS map.

5.3. Enhanced Total Horizontal Gradient of Tilt Angle (ETHDR)

Arisoy and Dikmen (2013) developed a new edge detection filter for the interpretation of magnetic data to overcome the problem of the dominance of high-amplitude anomalies obscuring subtle anomalies in the THDR and AS methods in the case of wide-range amplitudes. The proposed ETilt filter is given as the ratio of vertical derivative to the total horizontal derivative of AS:

$$\mathrm{ETilt} = \tan^{-1}\left[k\frac{\left(\frac{\partial H}{\partial z}\right)}{\sqrt{\left(\frac{\partial A}{\partial x}\right)^2+\left(\frac{\partial A}{\partial y}\right)^2}}\right]$$

$$\mathrm{ETHDR} = \sqrt{\left(\frac{\partial \mathrm{ETilt}}{\partial x}\right)^2+\left(\frac{\partial \mathrm{ETilt}}{\partial y}\right)^2}$$

where $k = \frac{1}{\sqrt{\Delta x^2+\Delta y^2}}$ is the dimensional correction factor, Δx and Δy are sampling intervals in the x and y direction, respectively,$\partial A/\partial x$, $\partial A/\partial y$ are the two horizontal derivatives of the AS, $\partial \mathrm{ETilt}/\partial x$, $\partial \mathrm{ETilt}/\partial y$ are the two horizontal derivatives of the ETilt.

ETHDR produces a very sharp gradient over the edges of the bodies making structural interpretation easier and more powerful. This method is an effective tool for delineating edges of shallow and deep structures in magnetic data.

ETHDR filter greatly amplifies noise in the data, so this was reduced as a first step by applying a low-pass filter to the RTP magnetic data. Figure 7a shows the results of applying an ETilt filter, whereas the ETHDR of RTP magnetic data can be seen in (Fig. 7b). High similarity in structural trends between THDR (Fig. 6a) and both Etilt and ETHDR (Fig. 7a, b, respectively) can be observed. Nevertheless, ETtilt and ETHDR filters produce higher resolution results, and are, therefore, more useful for constructing a structural map of the Mygdonian Basin. These maps present the same fault trends in N–S, NW–SE, and NE–SW directions.

6. Estimation of Depth to the Top of Magnetic Sources

6.1. Tilt Derivative (TDR)

The tilt derivative (TDR) of magnetic anomaly fields is a method for edge detection and depth estimation (Miller and Singh 1994; Verduzco et al. 2004; Oruç and Keskinsezer 2008; Pilkington and Tschirhart 2017).

$$\mathrm{TDR}(H) = \tan^{-1}\left(\frac{\partial H/\partial z}{\sqrt{(\partial H/\partial x)^2+(\partial H/\partial y)^2}}\right)$$

where $\partial H/\partial x$, $\partial H/\partial y$, $\partial H/\partial z$ are the first-order derivatives of the magnetic field in the x, y, and z direction, respectively.

The tilt derivative uses a range from $-\pi/2$ to $+\pi/2$ and has values close to zero above edges of the causative bodies, whereas high positive values are assumed to be located directly above magnetic sources (Verduzco et al. 2004). Salem et al. (2007) and Oruç (2011) used the half-distance between $-\pi/4$ and $\pi/4$ rad contours to calculate the depths to the top of the contact of magnetic sources. The TDR of RTP magnetic data in the survey area was calculated (Fig. 8) and the contour lines $-\pi/4$, 0 and $+\pi/4$ are also displayed. The dashed black line marks the edge of the contact and localizes the contact location. The dominant trends in the area are N–S, NW–SE, and NE–SW. The depths to the magnetic contacts were also calculated for chosen locations in the survey area and are presented in Table 2.

6.2. Source parameter imaging (SPI) technique

SPI is a procedure for the automatic calculation of source depths from gridded magnetic data. The depth solutions are independent of the magnetic inclination and declination, so it is not necessary to use a pole-

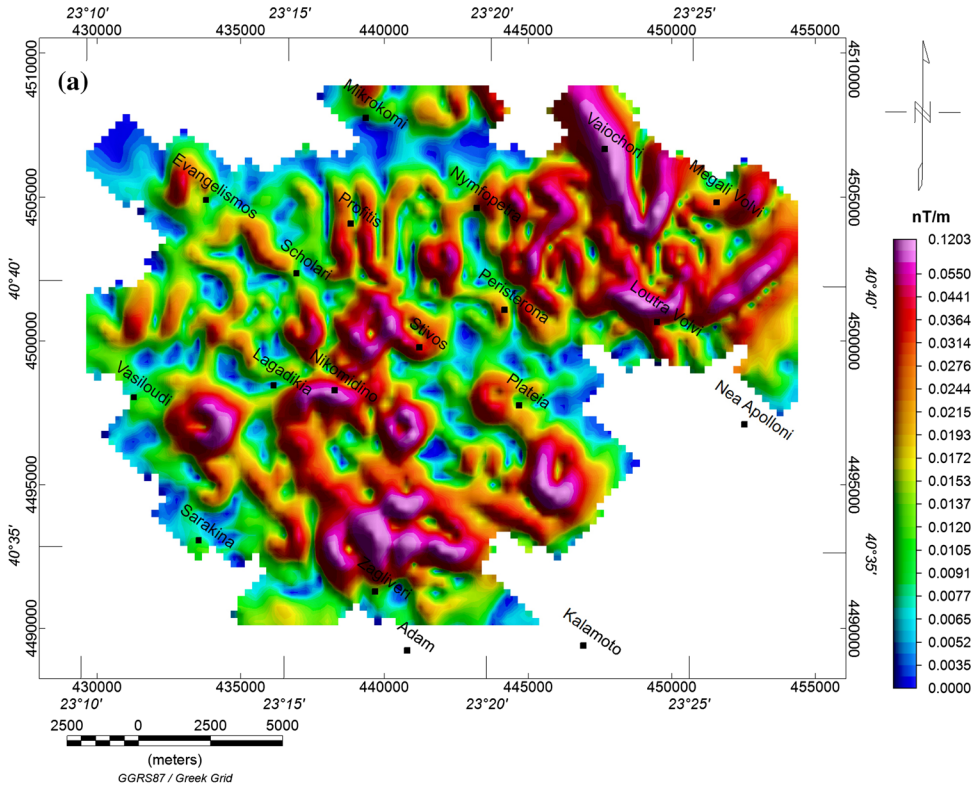
(a)
23°10′
23°15′
23°20′
23°25′
430000
435000
440000
445000
450000
455000
4510000
4505000
4500000
4495000
4490000
40°40′
40°35′
Mikrokomi
Vaiochori
Evangelismos
Nymfopetra
Megali Volvi
Profitis
Scholari
Peristerona
Loutra Volvi
Stivos
Lagadikia
Nikomidino
Vasiloudi
Platela
Nea Apolloni
Sarakina
Zagliveri
Adam
Kalamoto
nT/m
0.1203
0.0550
0.0441
0.0364
0.0314
0.0276
0.0244
0.0215
0.0193
0.0172
0.0153
0.0137
0.0120
0.0105
0.0091
0.0077
0.0065
0.0052
0.0035
0.0000
2500 0 2500 5000
(meters)
GGRS87 / Greek Grid

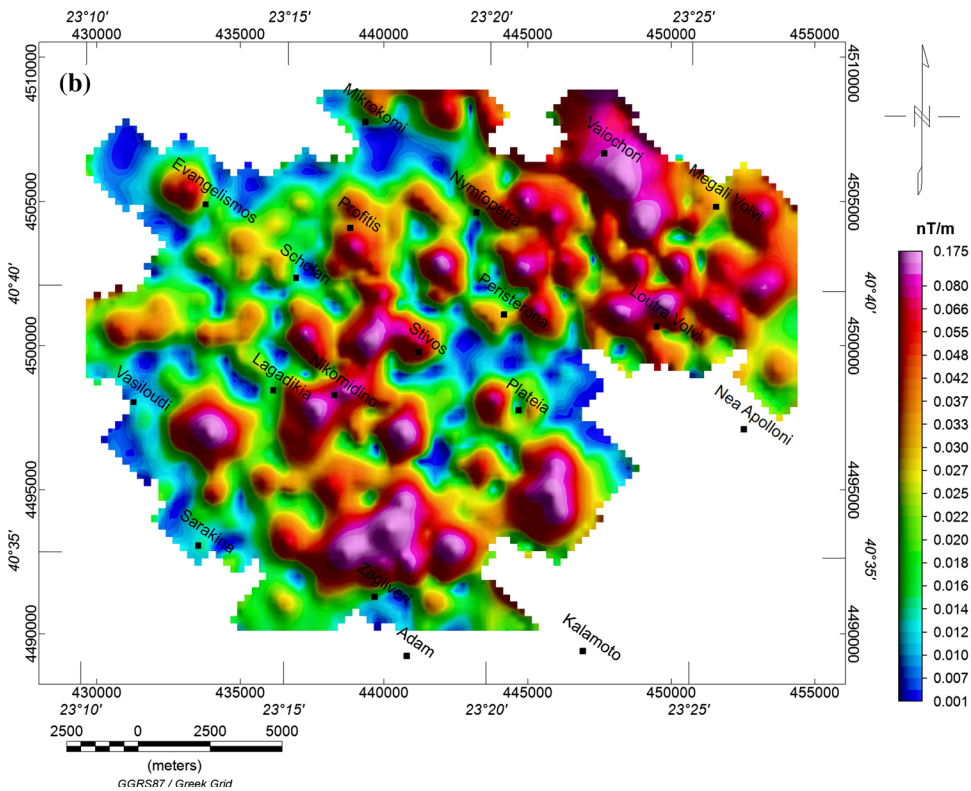
(b)
23°10′
23°15′
23°20′
23°25′
430000
435000
440000
445000
450000
455000
4510000
4505000
4500000
4495000
4490000
40°40′
40°35′
Mikrokomi
Vaiochori
Evangelismos
Nymfopetra
Megali Volvi
Profitis
Scholari
Peristerona
Loutra Volvi
Stivos
Lagadikia
Nikomidino
Vasiloudi
Platela
Nea Apolloni
Sarakina
Zagliveri
Adam
Kalamoto
nT/m
0.175
0.080
0.066
0.055
0.048
0.042
0.037
0.033
0.030
0.027
0.025
0.022
0.020
0.018
0.016
0.014
0.012
0.010
0.007
0.001
2500 0 2500 5000
(meters)
GGRS87 / Greek Grid

◀Figure 6
Total horizontal derivative (**a**) and analytical signal (**b**) maps of the RTP magnetic data of Mygdonian Basin

reduced input grid (Thurston and Smith 1997). This technique uses the Blakely and Simpson (1986) method to find localized peaks in a grid. For each grid cell to be considered, the routine compares its value with the eight surrounding grid cells in four directions (x-direction, y-direction, and both diagonals). The horizontal derivatives are computed perpendicular to the strike using the least squares method (Phillips et al. 2007).

SPI assumes a step-type source model. For a step, the following formula holds (Thurston and Smith 1997):

$$\text{Depth} = \frac{1}{K_{\max}}$$

where $K_{\max}$ is the peak value of the local wavenumber K over the step source.

$$K = \sqrt{\left(\frac{\partial A}{\partial x}\right)^2 + \left(\frac{\partial A}{\partial y}\right)^2}$$

$$A = \tan^{-1}\left[\frac{\left(\frac{\partial H}{\partial z}\right)}{\sqrt{\left(\frac{\partial H}{\partial x}\right)^2 + \left(\frac{\partial H}{\partial y}\right)^2}}\right]$$

where k *is* the local wavenumber (horizontal gradient of tilt derivative), H is the total magnetic field anomaly grid, and A is the tilt derivative. SPI first computes A and K, and then finds peak values $K_{\max}$ using the Blakely and Simpson (1986) algorithm. These peak values are used to compute depth solutions.

In the present study, the SPI technique was applied to the TMI grid. The estimated SPI depths in the survey area vary from a few meters to 590 m as shown in (Fig. 9). The depths estimated using this technique are in agreement with the depths obtained from the 2D power spectrum technique. The depths obtained from the TDR method are also within this range.

6.3. 2D Forward Modeling

Ambiguity in our forward magnetic modeling was reduced by applying some constraints such as the depth derived from the existing boreholes and/or susceptibilities of basement rocks. The susceptibility values for the sedimentary rocks are very low in comparison with igneous rocks which can be considered zero in regional studies, whereas the average susceptibility value for granitic rocks is $S = 0.004$ SI unit (Lowrie 2007).

2D forward modeling was carried out using the interactive GM-SYS modeling program (2013), a toolkit that is a part of Geosoft Oasis Montaj software, which was initially produced by Northwest Geophysical Associates Inc., based on the methods of Talwani et al. (1959), and Talwani and Heirtzler (1964) and using the algorithms described by Won and Bevis (1987). To avoid edge effects, 2D cross-sections are extended up to ± 30,000 km along the profile at its extremities.

In the present study, boreholes (Table 1), previous geological and structural information, results of depth estimation, and susceptibilities of the exposed rocks measured in the field were used as constraints for the initial models. Four profiles (Fig. 10) were selected to cover the basin area. The profiles were chosen to cut the strike of the basin as well as to pass through the existing boreholes which served as constraints for the depth of the basement surface. Polygonal model blocks were constructed to represent the subsurface geological units along each profile. By way of a manually iterated procedure, each structural unit or block was adjusted and/or magnetic susceptibility values were updated. Subsequently, the overall calculated (synthetic) geomagnetic response of the modeled two-layered magnetic susceptibility structures below each traverse was statistically compared to the observed geomagnetic response to satisfy a certain root-mean-square (RMS) data misfit (GM-SYS manual 2013). The deviation between the observed and calculated data at each station represents the fitting error. We found excellent model fit for all four profiles. The pertinent details of the 2D modeling sections of the four profiles are summarized in Table 3.

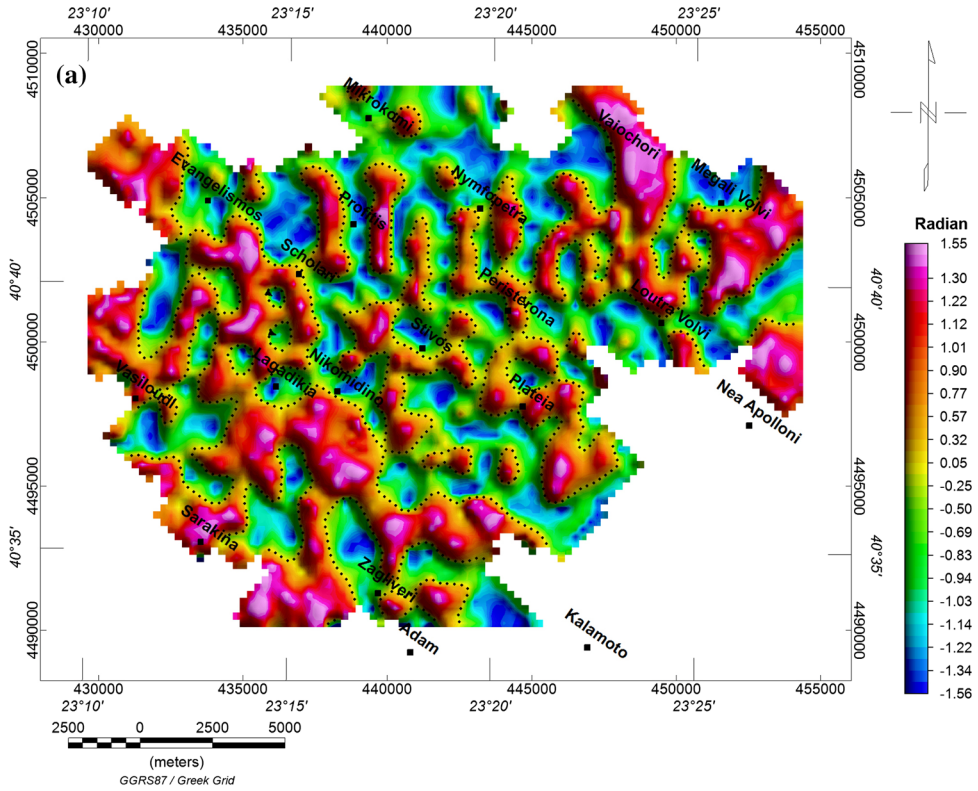
(a)
Mikrokomi
Vaiochori
Evangelismos
Nymfopetra
Megali Volvi
Protitis
Scholari
Peristerona
Loutra Volvi
Stivos
Lagadikia
Nikomidino
Vasiloudi
Platela
Nea Apolloni
Sarakina
Zagliveri
Adam
Kalamoto
Radian
1.55
1.30
1.22
1.12
1.01
0.90
0.77
0.57
0.32
0.05
-0.25
-0.50
-0.69
-0.83
-0.94
-1.03
-1.14
-1.22
-1.34
-1.56
23°10′
23°15′
23°20′
23°25′
40°40′
40°35′
2500 0 2500 5000
(meters)
GGRS87 / Greek Grid

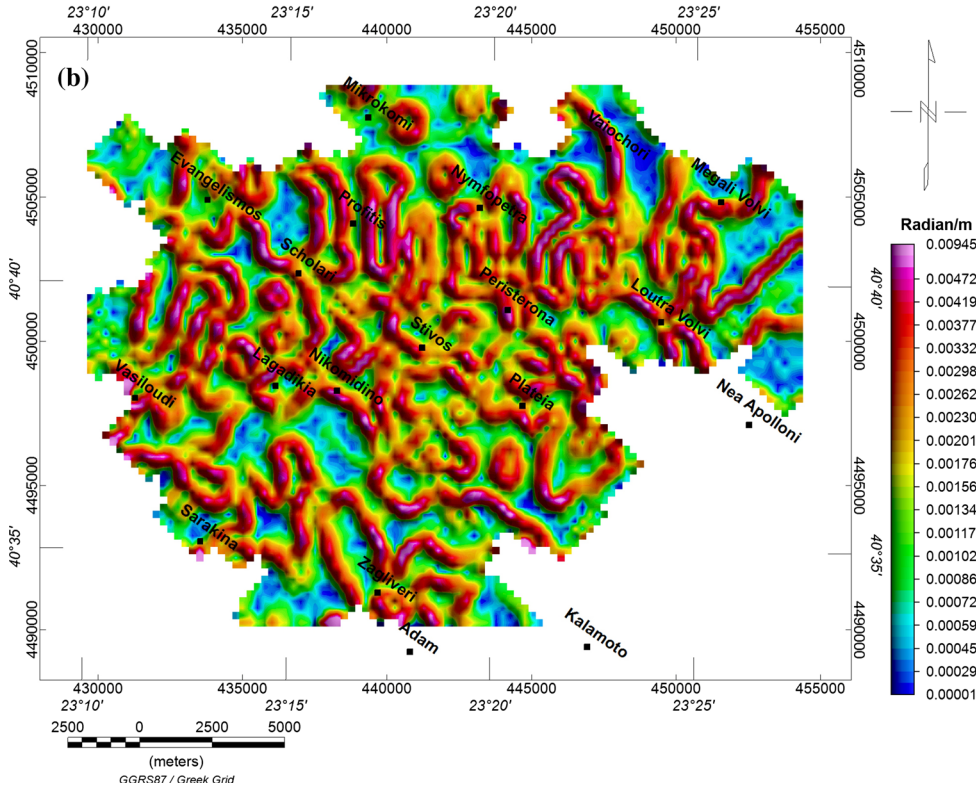
(b)
Mikrokomi
Vaiochori
Evangelismos
Nymfopetra
Megali Volvi
Protitis
Scholari
Peristerona
Loutra Volvi
Stivos
Lagadikia
Nikomidino
Vasiloudi
Platela
Nea Apolloni
Sarakina
Zagliveri
Adam
Kalamoto
Radian/m
0.00945
0.00472
0.00419
0.00377
0.00332
0.00298
0.00262
0.00230
0.00201
0.00176
0.00156
0.00134
0.00117
0.00102
0.00086
0.00072
0.00059
0.00045
0.00029
0.00001
23°10′
23°15′
23°20′
23°25′
40°40′
40°35′
2500 0 2500 5000
(meters)
GGRS87 / Greek Grid

◀Figure 7
ETilt **(a)** and ETHDR **(b)** maps of the RTP magnetic data of Mygdonian Basin. A zero radian contour is represented on the ETilt map by dotted lines

7. *Summary and Discussion*

In this study, several techniques were used to explore the structural architecture of the Mygdonian Basin and to determine the distribution of the sedimentary cover. RTP magnetic data were transformed into the frequency domain using FFT. The power spectrum was calculated and its segments were determined. The high frequency component (beyond Nyquist frequency) in the magnetic data was removed by applying a low-pass filter with a cutoff wavenumber of 1 km^{-1}. Low-pass filtered regional and high-pass filtered residual components were separated using low- and high-pass filters with a cutoff wavenumber of 0.17 km^{-1}.

The depth to the basement was calculated using the following methods: averaged power spectrum, SPI, TDR as well as 2D forward magnetic modeling. Depths derived from TDR coincided well with the depth information obtained from available boreholes and previous studies which assumed a depth range of 0–400 m inside the basin. Spectrum analysis and SPI methods suggest the same depths in the basin, but a

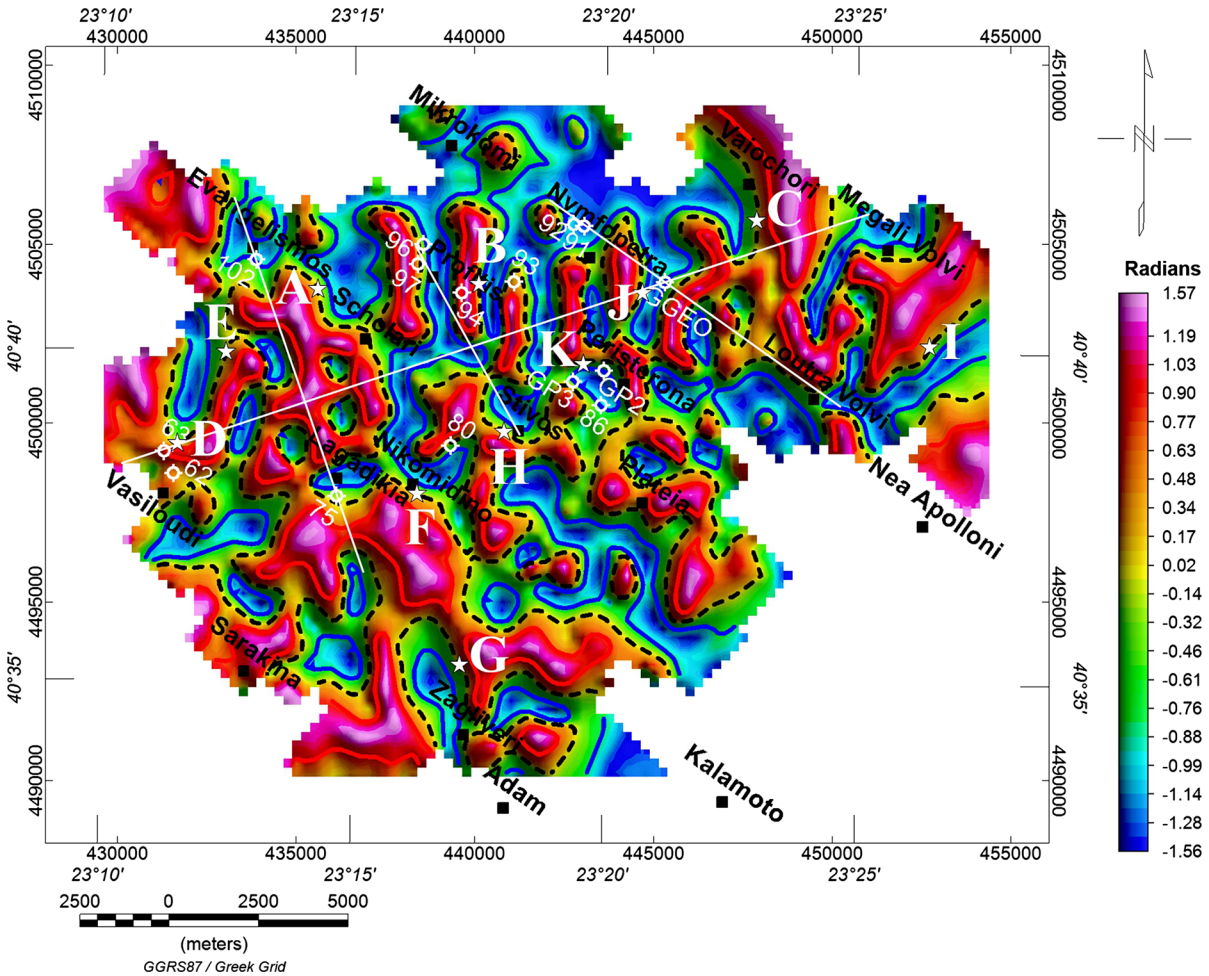

Figure 8
TDR of RTP magnetic data of Mygdonian Basin. The dashed black lines represent the zero radian contour of TDR whereas blue and red lines represent $-\pi/4$ to $+\pi/4$ rad contour lines, respectively. White stars with letters (A,B,…,K) demonstrate the locations of depth estimations

Table 2

Results of depth estimation using TDR method

Label	*X*	*Y*	Depth (m)
A	435,605	4,503,638	330
B	440,080	4,503,900	160
C	447,884	4,505,880	400
D	431,607	4,499,380	150
E	432,949	4,501,754	390
F	438,356	4,498,017	325
G	439,540	4,493,265	380
H	440,855	4,499,746	210
I	452,785	4,502,209	375
J	444,695	4,503,780	158
K	442,995	4,501,607	187

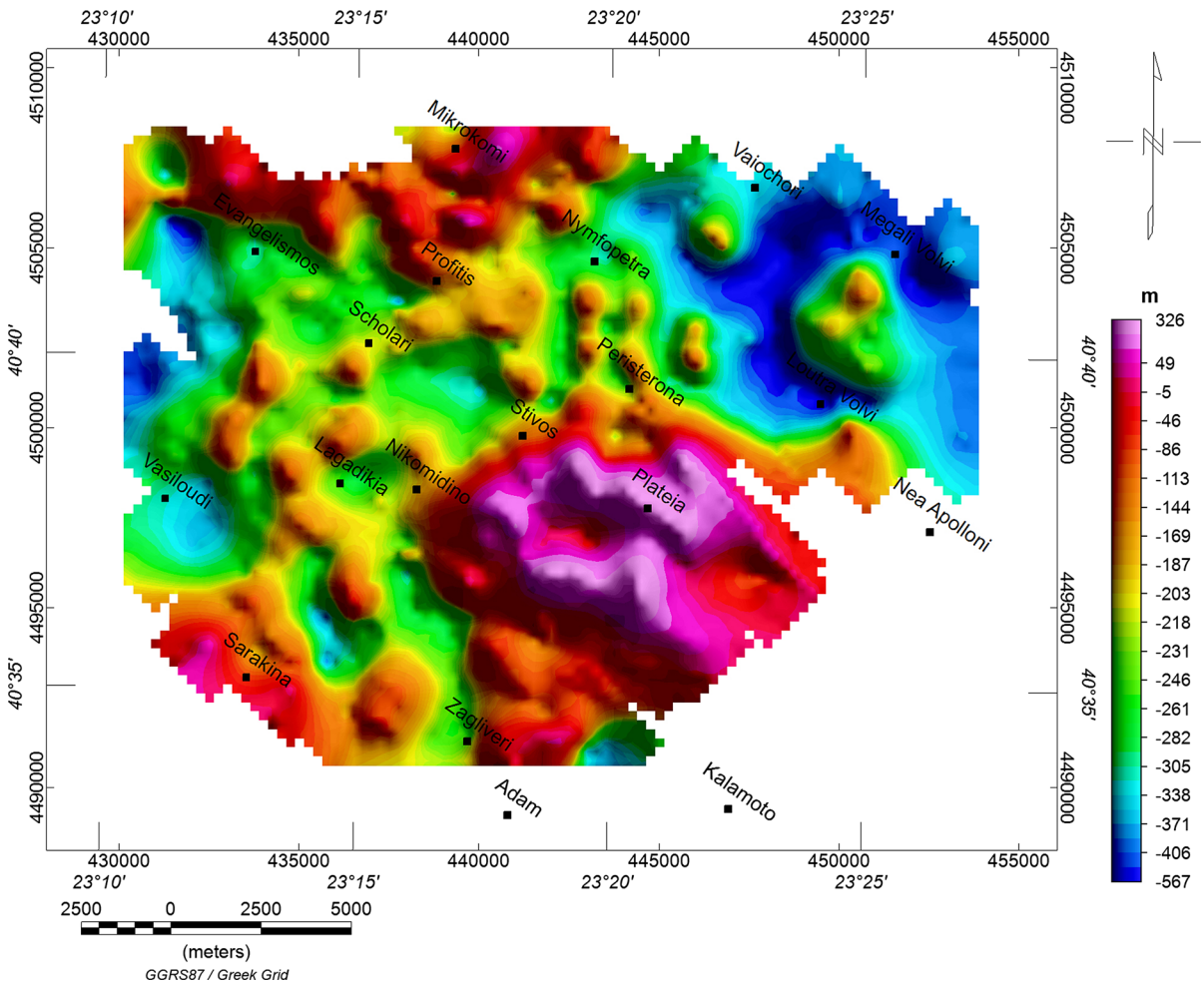

Figure 9
Depth to magnetic sources based on SPI technique (from sea level)

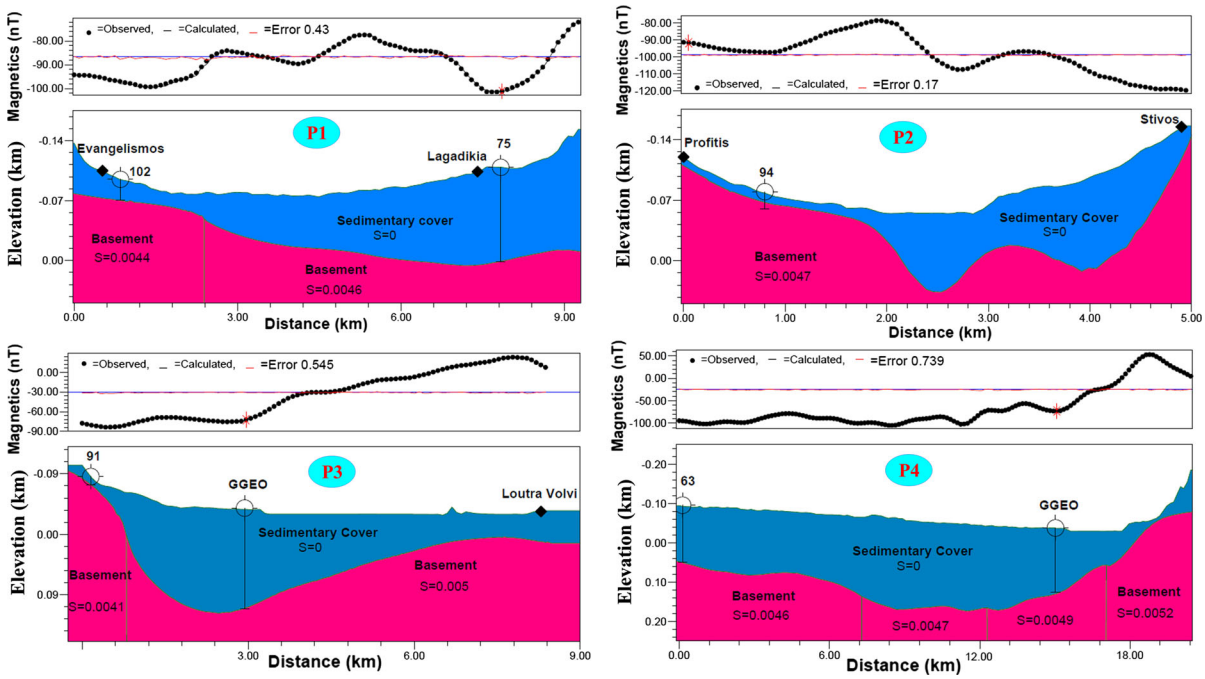

Figure 10
2D forward models of the four transects through the Mygdonian Basin. Refer to Fig. 4 for the location of the transects and boreholes and to Table 1 for the information about boreholes

Table 3

Description of the 2D magnetic modeling sections

Profile	Azimuth	Length (m)	Susceptibility SI unit	Constraining boreholes	Description of 2D section
P1	161	9250	0.0044–0.0046	102 75	The thickness of the sediments increases from 10 m at the south of Evangelismos to more than 150 m at Lagadikia
P2	151	4950	0.0047	96 97 94	An abrupt increase in the basement depth from 0 m to the south of Stivos to 115 m to the north suggests that the fault F-GNSP may be seen at this place. This agrees with the available structural information (see Fig. 2). Two grabens and one horst are evident along this profile
P3	125	8375	0.0041–0.0050	91 92 GGEO	The depth to the basement ranges between less than 10 m at the north of Nymfopetra to more than 160 m at the east of it. A fault with a throw to SE direction was determined northwest of Nymfopetra based on an inspection of the rapid change in the magnetic field (Fig. 4b) and in the cross-section of profile P3
P4	71.5	20,450	0.0046–0.0052	62 63 GGEO	The range of sedimentary cover along this profile is 15–250 m

deeper depth of about 600 m in the area of Lake Langada and Lake Volvi. Deviations in depth estimation occur, because the SPI and power spectrum methods calculate depth at each point on the magnetic grid, whereas the TDR and 2D forward magnetic modeling methods calculate depth at preselected points or profiles. As a comparison between the depth estimation from the TDR (Fig. 8) and 2D forward modeling techniques, we calculated the depths to the basement at locations D (150 and

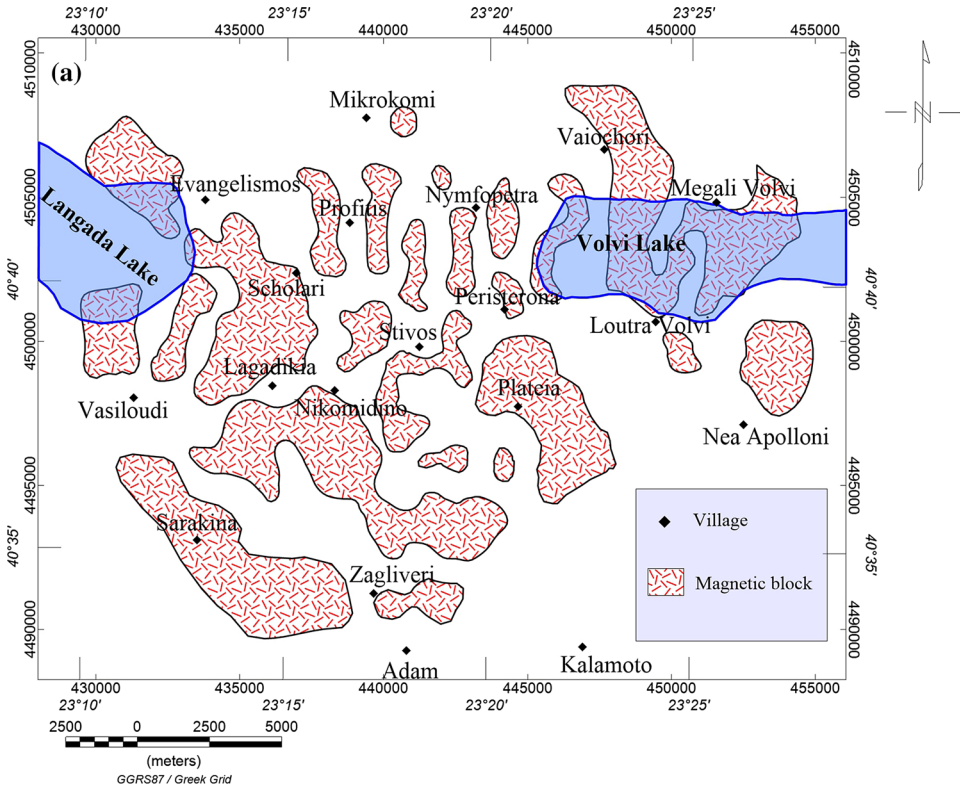
(a)
Mikrokomi
Vaiochori
Evangelismos
Profitis
Nymfopetra
Megali Volvi
Langada Lake
Volvi Lake
Scholari
Peristerona
Loutra Volvi
Stivos
Lagadikia
Plateia
Vasiloudi
Nikomidino
Nea Apolloni
Sarakina
Zagliveri
Adam
Kalamoto
Village
Magnetic block
23°10′
23°15′
23°20′
23°25′
40°40′
40°35′
2500 0 2500 5000
(meters)
GGRS87 / Greek Grid

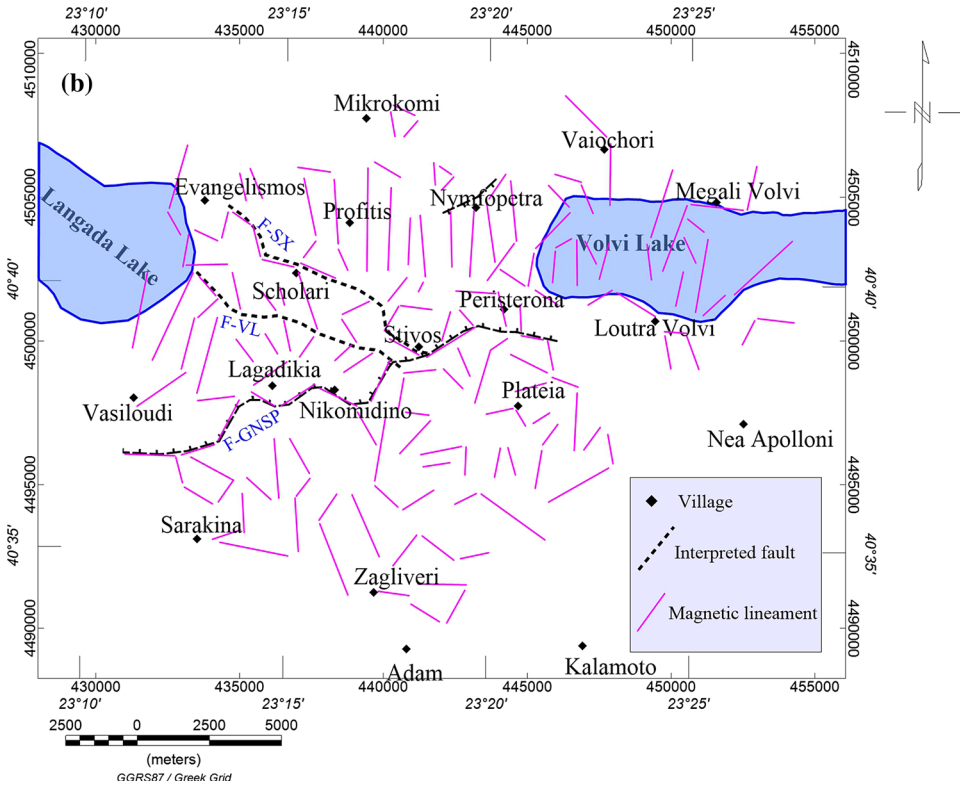
(b)
Mikrokomi
Vaiochori
Evangelismos
Profitis
Nymfopetra
Megali Volvi
Langada Lake
Volvi Lake
F-SX
Scholari
Peristerona
F-VL
Loutra Volvi
Stivos
Lagadikia
Plateia
Vasiloudi
Nikomidino
F-GNSP
Nea Apolloni
Sarakina
Zagliveri
Adam
Kalamoto
Village
Interpreted fault
Magnetic lineament
23°10′
23°15′
23°20′
23°25′
40°40′
40°35′
2500 0 2500 5000
(meters)
GGRS87 / Greek Grid

◀Figure 11
Interpreted magnetic blocks (**a**) and magnetic faults/lineaments (**b**)

147 m, respectively) and J (178 and 170 m, respectively). The depth to the basement at location K calculated by the TDR method was 187 m, whereas 180 m was measured at the nearby borehole GP2.

The profile between Stivos and Profitis (P2) can be seen as a reference, as it has already been studied intensively using seismic, geoelectric (Tournas 2005; Manakou et al. 2010), and electromagnetic methods (Gurk et al. 2008; Bastani et al. 2011; Autio et al. 2016; Widodo et al. 2016). All of these methods suggest a similar basement topography to our 2D magnetic model. Nevertheless, the magnetic and electromagnetic data imply a basement uplift at a distance around 1.5 km north of Stivos that can be associated to possible normal faults. We constrained our 2D modeling with borehole information. The central section of profile P2 suggests a slightly less deep basement compared to other methods.

Our general findings were more pronounced towards the transition to the CRB in the western part of the survey area. Here we found a magnetic high that contrasts with the sediment thickness published by Gurk et al. (2008) and Manakou et al. (2010). Our model suggests the extension of sediments towards the southeast, underneath the village of Lagadikia.

A detailed interpreted structural map (Fig. 11a) was constructed using all previous results showing the structural architecture of the Mygdonian Basin. The dominant structural trends inferred from the lineament analysis of magnetic maps (regional, residual, THDR, AS, TDR, and ETHDR) are N–S, NW–SE, NE–SW, and E–W. These trends correspond well with the known geological and previous geophysically deduced directions, which have played an important role in the basin's evolution. We may assume that known tufa outcrops in the north of the area are associated with predominant lineaments in the magnetic basement. Based on the results of the TDR technique (Fig. 8), the magnetic sources were traced and then the magnetic blocks (Fig. 11b) were inferred.

8. Conclusions

The magnetic method proved a powerful tool in mapping the basement surface in the Mygdonian Basin. It can be concluded that the dominant structural trends in the Mygdonian Basin are N–S, NW–SE, NE–SW, and E–W. These trends have played an important role in the basin′s evolution. We believe that the N–S trend is affecting the shallow depths of the area and could presently be an extension pattern in the basement. We also found that the depth to the basement inside the basin ranges from 0 to 400 m, and increases up to 600 m in the area of Lake Langada and Lake Volvi. Moreover, a detailed map of magnetic blocks was created based on the results of the TDR technique.

For geothermal explorations, we suggest that the area around the western part of Lake Volvi and also the horst-type structure between Profitis and Stivos is worthy of geothermal investigation. These kinds of structures are very good at concentrating and storing geothermal resource, especially near faults and on top of horsts. Furthermore, there is evidence of geothermal activity in the area, such as tufa towers and hot springs.

The marine survey on Lake Volvi extended the geophysical survey of the Mygdonian Basin towards the east for the first time. Based on our findings, we would recommend the execution of marine electromagnetic (Bastani et al. 2015) and magnetic surveys to map entire of Lake Volvi and its surrounding area.

Finally, edge detection and depth estimation techniques used in this study have provided an invaluable contribution to the understanding of the structural and tectonic framework as well as basement depth distribution in the Mygdonian Basin. In the future, we strongly suggest performing 3D magnetic modeling and joint interpretation with available seismic and electromagnetic data.

Acknowledgements

The study was supported by the Marie Curie Reintegration Grant IGSEA—Integrated Nonseismic Geophysical Studies to Assess the Site Effect of the EUROSEISTEST Area in Northern Greece—

PERG03-GA-2008-230915 {REF RTD REG/T.2 (2008)D/596232}, the School of Geology of the Aristotle University of Thessaloniki and the Institute of Engineering Seismology and Earthquake Engineering (ITSAK) in Thessaloniki. We thank Professor Konstantinos Albanakis, Dr. Alexandros Savvaidis, Dr. Juliane Adrian, and Dr. Hannah Langenbach and many of our colleagues for their support. We also thank two anonymous reviewers and Editor Nils Olsen for their constructive comments that have greatly improved the manuscript. The first author is hugely indebted to the Institute of International Education (IIE)—USA and to the University of Cologne for hosting him as a postdoctoral academic visitor.

References

Arisoy, M. Ö., & Dikmen, Ü. (2013). Edge detection of magnetic sources using enhanced total horizontal derivative of tilt angle. *Bulletin of the Earth Sciences Application and Research Center of Hacettepe University, 34*(1), 73–82.

Autio, U., Smirnov, M Yu., Savvaidis, A., Soupios, P., & Bastani, M. (2016). Combining electromagnetic measurements in the Mygdonian sedimentary basin, Greece. *Journal of Applied Geophysics, 135,* 261–269.

Bastani, M., Persson, L., Mehta, S., & Malehmir, A. (2015). Boat towed radio-magnetotellurics—A new technique and case study from the city of Stockholm. *Geophysics, 80,* B193–B202.

Bastani, M., Savvaidis, A., Pedersen, L. B., & Kalscheuer, T. (2011). CSRMT measurements in the frequency range of 1–250 kHz to map a normal fault in the Volvi basin, Greece. *Journal of Applied Geophysics, 75,* 180–195.

Bhattacharyya, B. K. (1965). Two dimensional harmonic analysis as a tool for magnetic interpretation. *Geophysics, 30*(5), 829–857.

Bhattacharyya, B. K. (1966). Continuous spectrum of the total magnetic field anomaly due to a rectangular prismatic body. *Geophysics, 31,* 97–121.

Blakely, R. J., & Simpson, R. W. (1986). Approximating edges of source bodies from magnetic or gravity anomalies. *Geophysics, 51,* 1494–1498.

BRGM, (1971). Etude Hydrogeologique du Basin de Mygdonia, O.A.E.S (in French).

Cassano, E., & Rocca, F. (1975). Interpretation of magnetic anomalies using spectral estimation techniques. *Geophysical Prospecting, 23*(4), 663–681.

Cheng, S., Fang, Z., Pavlides, S., & Chatzipetros, A. (1994). Preliminary study of the paleoseismicity of the southern Langada-Volvi Basin margin fault zone, Thessaloniki, Greece. *Bulletin of the geological society of Greece, xxx*(1), 401–407.

Connard, G., Couch, R., & Gemperle, M. (1983). Analysis of aeromagnetic measurements from the Cascade Range in central Oregon. *Geophysics, 48*(3), 376–390.

Cordell, L., & Grauch, V. J. S. (1985). Mapping basement magnetization zones from aeromagnetic data in the San Juan Basin, New Mexico. In W. J. Hinze (Ed.), *The utility of regional gravity and magnetic anomaly maps* (pp. 181–197). Tulsa: Society of Exploration Geophysics.

Dewey, J. F., & Sengör, A. M. (1979). Aegean and surrounding regions: complex multiplate and continuum tectonics in a convergent zone. *Geological Society of America Bulletin, 90*(1), 84–92.

Fedi, M., Quarta, T., & De Santis, A. (1997). Inherent power—law behavior of magnetic field power spectra from Spector and Grant ensemble. *Geophysics, 62*(4), 1143–1150.

Geosoft Oasis Montaj. (2008). *Data processing and analysis systems for earth science applications (Ver. 7)*. Toronto: Geosoft Inc.

GM-SYS. (2013). *A Gravity and Magnetic Modeling Software Part of the Oasis Montaj Software Suite 7*. Toronto: Geosoft Inc.

Gurk, M., Smirnov, M.Yu., Savvaidis, A., Pedersen, L. B., & Ritter, O., (2008). A 3D Magnetotelluric study of the basement structure in the Mygdonian Basin (Northern Greece). In O. Ritter, H. Brasse (eds) *Protokoll über das Kolloquium: Elektromagnetische Tiefenforschung, in Hotel Maxičky, Děčín, Czech Republic*, 1–5 October 2007 (pp. 231–238).

Hancock, P. L., Chalmes, R. M. L., Altunel, E., & Cakir, Z. (1999). Travitonics: using travertines in active fault studies. *Journal of Structural Geology, 21,* 903–916.

Hatzfeld, D., Christodoulou, A. A., Scordilis, E. M., Panagiotopoulos D., & Hatzidimitriou, P. M. (1987). A microearthquake study of the Mygdonian graben (northern Greece). In *Earth and Science Letters* (vol. 81, No. 1986/87, pp. 379–396). Amsterdam: Elsevier Science Publishers B.V.

Hinze, W. J., Von Frese, R. R. B., & Saad, A. H. (2013). *Gravity and magnetic exploration: principles, practices, and applications*. Cambridge: Cambridge University Press.

Ibraheem, I. M., Elawadi, E. A., & El-Qady, G. M. (2018). Structural interpretation of aeromagnetic data for the Wadi El Natrun area, northwestern desert, Egypt. *Journal of African Earth Sciences, 139,* 14–25. https://doi.org/10.1016/j.jafrearsci.2017.11.036.

Jacobshagen, V. (1986). *Geologie von griechenland* (pp. 1–163). Berlin: Gebrüder Borntraeger.

Karagianni, E. E., Panagiotopoulos, D. G., Papazachos, C. B., & Burton, P. W. (1999). A study of shallow crustal structure in the Mygdonia Basin (N. Greece) based on the dispersion curves of Rayleigh waves. *Journal of the Balkan Geophysical Society, 2*(1), 3–14.

Kockel, F., Mollat, H., & Walther, H. W. (1971). Geologie des Serbo-Mazedonischen Massivs und seines mesozoischen Rahmens (Nordgriechenland). *Geologisches Jahrbuch, 89,* 529–551.

Lowrie, M. (2007). *Fundamentals of geophysics*. New York: Cambridge University Press.

Makra, K., & Chavez-Garcia, F. J. (2016). Site effects in 3D basins using 1D and 2D models: an evaluation of the differences based on simulations of the seismic response of Euroseistest. *Bulletin of Earthquake Engineering, 14*(4), 1177–1194.

Manakou, M., Raptakis D., Apostolidis P., Chavez-Garcia F. J., & Pitilakis, K. (2007). *The 3D geological structure of the Mygdonian sedimentary Basin (Greece)*. 4th International Conference on Earthquake Geotechnical Engineering, June 25–28. Paper No. 1686.

Manakou, M. V., Raptakis, D. G., Chavez-Garcia, F. J., Apostolidis, P. I., & Pitilakis, K. D. (2010). 3D soil structure of the Mygdonian Basin for site response analysis. *Soil Dynamics and Earthquake Engineering, 30*(11), 1198–1211.

Marson, I., & Klingele, E. E. (1993). Advantages of using the vertical gradient of gravity for 3-D interpretation. *Geophysics, 58*(11), 1588–1595.

Miller, H. G., & Singh, V. (1994). Potential field tilt—A new concept for location of potential field sources. *Journal of Applied Geophysics, 32*(2–3), 213–217.

Oruç, B. (2011). Edge detection and depth estimation using a tilt angle map from gravity gradient data of the Kozaklı-Central Anatolia region, Turkey. *Pure and Applied Geophysics, 168*(10), 1769–1780. https://doi.org/10.1007/s00024-010-0211-0.

Oruç, B., & Keskinsezer, A. (2008). Structural setting of the northeastern Biga Peninsula (Turkey) from tilt derivatives of gravity gradient tensors and magnitude of horizontal gravity components. *Pure and Applied Geophysics, 165*(9–10), 1913–1927. https://doi.org/10.1007/s00024-008-0407-8.

Phillips, J. D. (1998). Processing and interpretation of aeromagnetic data for the Santa Cruz Basin-Patahonia Mountains area, South-Central Arizona. U. S. Geological Survey Open-File Report, 02-98.

Phillips, J. D., Hasen, R. O., & Blakely, R. J. (2007). The use of curvature in potential field interpretation. *Exploration Geophysics, 38,* 111–119.

Pilkington, M., & Tschirhart, V. (2017). Practical considerations in the use of edge detectors for geological mapping using magnetic data. *Geophysics, 82*(3), J1–J8. https://doi.org/10.1190/geo2016-0364.1.

Psilovikos, A. (1977). Paleographic development of the basin and Lake of Mygdonia (Langada-Volvi area, Greece). Ph.D. Thesis, University of Thessaloniki.

Psilovikos, A., & Sotiriadis, L. (1983). The neotectonic graben complex of the Serbomacedonian massif at the area of Promygdonia Basin in northern Greece. *Clausthaler Geologische Abhandlungen, 44,* 21–53.

Raptakis, D. G., Manakou, M. V., Chavez-Garcia, F. J., Makra, K. A., & Pitilakis, K. D. (2005). 3D configuration of Mygdonian Basin and preliminary estimate of its site response. *Soil Dynamics and Earthquake Engineering, 25,* 871–887.

Saade, S. A. (2016). Edge detection and depth estimation of Galala El Bahariya Plateau, Eastern Desert-Egypt, from aeromagnetic data. *Geomechanics and Geophysics for Geo-Energy and Geo-Resources, 2*(1), 25–41. https://doi.org/10.1007/s40948-015-0019-6.

Salem, A., Williams, S., Fairhead, J. D., Ravat, D., & Smith, R. (2007). Tilt-depth method: A simple depth estimation method using first-order magnetic derivatives. *The Leading Edge, 26,* 1502–1505.

Spector, A., & Grant, F. S. (1970). Statistical models for interpretation aeromagnetic data. *Geophysics, 35,* 293–302.

Stampolidis, A., & Tsokas, G. N. (2002). Curie point depths of Macedonia and Thrace, N. Greece. *Pure and Applied Geophysics, 159,* 2659–2671. https://doi.org/10.1007/s00024-002-8752-5.

Talwani, M., & Heirtzler, J. R. (1964). Computation of magnetic anomalies caused by two-dimensional bodies of arbitrary shape. in G. A. Parks (Ed.), *Computers in the mineral industries*, Part 1, Stanford University Publications, Geological Sciences, 9, 464-480.

Talwani, M., Warzel, J. L., & Landisman, M. (1959). Rapid gravity computation for two-dimensional bodies with application to the Mendocino submarine fracture zone. *Journal of Geophysical Research, 64*(1), 49–59.

Thanassoulas, C., Tselentis, G.-A., & Traganos, G. (1987). A preliminary resistivity investigation (VES) of the Langada hot springs area in northern Greece. *Geothermics, 16*(3), 227–238.

Thurston, J. B., & Smith, R. S. (1997). Automatic conversion of magnetic data to depth, dip and susceptibility contrast using the SPI™ method. *Geophysics, 62*(3), 807–813.

Tournas, D. (2005). Study of the geometry of the Mygdonian Basin in the area of the European Test Site with geophysical methods. MSc. thesis, Aristotle University, Thessaloniki, (in Greek).

Tranos, M. D., Papadimitriou, E. E., & Kilias, A. A. (2003). Thessaloniki-Gerakarou Fault Zone (TGFZ): The western extension of the 1978 Thessaloniki earthquake fault (Northern Greece) and seismic hazard assessment. *Journal of Structural Geology, 25*(12), 2109–2123.

Veranis, N. (2010). Hydrogeological study of the Granular aquifer system of Mygdonia. Un. report IGME, Thessaloniki, maps, sections.

Verduzco, B., Fairhead, J. D., Green, C. M., & MacKenzie, C. (2004). New insights into magnetic derivatives for structural mapping. *The Leading Edge, 23*(2), 116–119. https://doi.org/10.1190/1.1651454.

Widodo, W., Gurk, M., & Tezkan, B. (2016). Multi-dimensional interpretation of radiomagnetotelluric and transient electromagnetic data to study active faults in the Mygdonian Basin, Northern Greece. *Journal of Environmental and Engineering Geophysics, 21*(3), 121–133. https://doi.org/10.2113/JEEG21.3.121.

Won, I. J., & Bevis, M. (1987). Computing the gravitational and magnetic anomalies due to a polygon: Algorithms and FORTRAN subroutines. *Geophysics, 52*(2), 232–238. https://doi.org/10.1190/1.1442298.

(Received August 8, 2017, revised February 9, 2018, accepted February 18, 2018, Published online February 23, 2018)